THE JOURNAL OF BIOLOGICAL CHEMISTRY VOL. 289, NO. 47, pp. 32871–32882, November 21, 2014
Published in the U.S.A.

Conformational Rearrangements in the Pro-apoptotic Protein, Bax, as It Inserts into Mitochondria

*A CELLULAR DEATH SWITCH**

Received for publication, July 2, 2014, and in revised form, October 9, 2014 Published, JBC Papers in Press, October 14, 2014, DOI 10.1074/jbc.M114.593897

Robert F. Gahl, Yi He, Shiqin Yu, and Nico Tjandra[1]

From the Laboratory of Molecular Biophysics, Biochemistry and Biophysics Center, National Heart, Lung and Blood Institute, National Institutes of Health, Bethesda, Maryland 20892

Background: The translocation of pro-apoptotic protein Bax from the cytosol to the mitochondria signals the commitment to cell death.
Results: Distances between locations in Bax were measured during translocation in live cells.
Conclusion: The conformational changes that coincide with the commitment to apoptosis were identified.
Significance: This information is crucial for the development of more effective therapeutics that target apoptosis.

The B-cell lymphoma 2 (Bcl-2) family of proteins regulates the activation of apoptosis through the mitochondria pathway. Pro- and anti-apoptotic members of this family keep each other in check until the correct time to commit to apoptosis. The point of no return for this commitment is the permeabilization of the outer mitochondrial membrane. Translocation of the pro-apoptotic member, Bax, from the cytosol to the mitochondria is the molecular signature of this event. We employed a novel method to reliably detect Förster resonance energy transfer (FRET) between pairs of fluorophores to identify intra-molecular conformational changes and inter-molecular contacts in Bax as this translocation occurs in live cells. In the cytosol, our FRET measurement indicated that the C-terminal helix is exposed instead of tucked away in the core of the protein. In addition fluorescence correlation spectroscopy (FCS) showed that cytosolic Bax diffuses much slower than expected, suggesting possible complex formation or transient membrane interaction. Cross-linking the C-terminal helix (α9) to helix α4 reduced the potential of those interactions to occur. After translocation, our FRET measurements showed that Bax molecules form homo-oligomers in the mitochondria through two distinct interfaces involving the BH3 domain (helix α2) and the C-terminal helix. These findings have implications for possible contacts with other Bcl-2 proteins necessary for the regulation of apoptosis.

Apoptosis is a critical mechanism in mammalian cells for maintaining tissue homeostasis, development, and immunity (1). A complex network of proteins and signals ensures that cells grow and replicate until a defined time where they are replaced by new cells. Disruption in this mechanism can lead to neurodegenerative, cancerous, or autoimmune diseases, (1–3). The Bcl-2 family of proteins is primarily responsible for initiating apoptosis through an intrinsic (mitochondria) pathway, where signals directly sensed by the cells can initiate the cascade of events that lead to a commitment to cell death (3, 4). This commitment culminates in the permeabilization of the outer mitochondrial membrane (OMM).[2] As a result, factors are released from the mitochondria that trigger downstream signaling for apoptosis including the activation of caspases (1, 5). Therefore, different steps that lead to the permeabilization of the OMM have been attractive therapeutic targets (6) to either initiate apoptosis in cancerous cells, or inhibit a constitutive activation present in autoimmune or degenerative diseases.

Each member of the Bcl-2 family of proteins can be classified as having pro- or anti-apoptotic activity (7) based on how they influence permeabilization of the OMM. Essential to OMM permeabilization is the activity of the pro-apoptotic member Bax. Bax mostly resides in the cytosol of healthy cells but translocates to the mitochondria where it mediates the permeabilization of the OMM. Interactions between Bax and other anti-apoptotic members such as Bcl-2 and Bcl-x_L have been shown to prevent OMM permeabilization (8).

Although these proteins have opposing functions, they are structurally homologous and have four conserved domains (BH). In addition, there is a subclass of pro-apoptotic proteins that only contains one homology domain, BH3, which has been thought to catalyze or disrupt interactions between the pro- and anti-apoptotic members (1). Despite knowing these features about the Bcl-2 family, the roles of these domains within a conserved mechanism to commit to apoptosis has yet to be elucidated (9). Therefore, identifying the conformational changes that Bax undertakes at the onset of the permeabilization of the OMM will go a long way in understanding how the Bcl-2 family regulates apoptosis. However, detecting these changes is not without challenges.

Conformational changes in Bax can only be identified as having regulatory consequences when the measurements are

* This work was supported by the Intramural Research Program of the National Institutes of Health, NHLBI.
[1] To whom correspondence should be addressed: 50 South Dr., Bldg. 50, Rm. 3503 Bethesda, MD 20892-8013. Tel.: 301-402-3029; Fax: 301-402-3405; E-mail: tjandran@nhlbi.nih.gov.

[2] The abbreviations used are: OMM, outer mitochondrial membrane; BH3, Bcl-2 homology domain 3; STS, staurosporin; FCS, fluorescence correlation spectroscopy; MEF, mouse embryonic fibroblast; eGFP, enhanced green fluorescent protein.

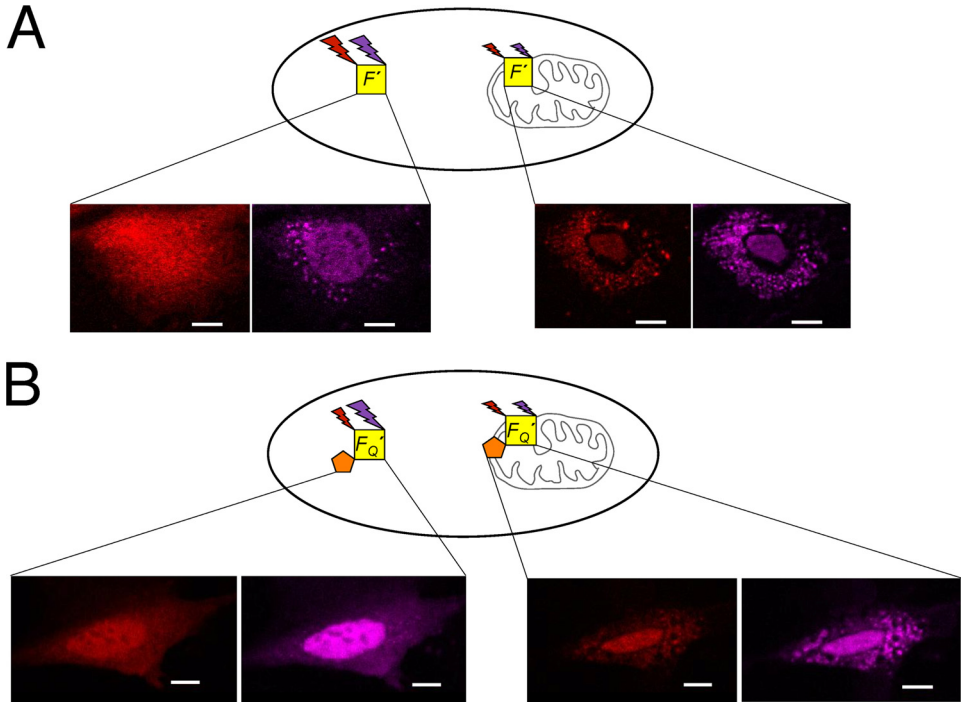

FIGURE 1. **A schematic diagram illustrating the utilization of a fluorescent internal reference to detect FRET between Alexa Fluor 546 and Dabcyl during translocation.** *A,* the fluorescence intensities of Bax (*F′*) conjugated with the FRET donor (Alexa Fluor 546, *red*) and the internal reference (Alexa Fluor 633, *purple*) are measured during translocation. *B,* the fluorescence intensities of another Bax sample, F_Q′, that contains the same FRET donor (*red*) and internal reference (*purple*) in addition to the non-fluorescent FRET acceptor (Dabcyl, *orange*) are also measured during translocation. Comparison of the relative intensities of the donor and internal reference with, F_Q′, and without, *F′*, the acceptor under similar conditions would provide FRET efficiency. All *scale bars* are 10 μm.

acquired under conditions where it is engaged in interactions with other members of the Bcl-2 family. In fact recent findings showed a dynamic equilibrium between cytosolic and mitochondria-associated Bax in healthy cells (10–12). Furthermore, over-expression of the anti-apoptotic protein Bcl-x_L was shown to shift this equilibrium toward the cytosolic population (10, 12). Therefore, this equilibrium is an important checkpoint in the commitment to engage in the permeabilization of the OMM. Valuable insight into the regulation of apoptosis can be obtained from extracting structural information about Bax under these conditions. This requires the acquisition of measurements in live cells before and after the initiation of apoptosis.

We monitor conformational changes in Bax associated with its translocation from the cytosol to the mitochondria resulting from the initiation of apoptosis using staurosporin (STS) in live mouse embryonic fibroblast (MEF) cells. Förster resonance energy transfer (FRET) was utilized to detect conformational changes between two fluorescence probes at different locations on Bax relative to the BH3 domain (helix α2). To circumvent the challenges of acquiring FRET measurements in the heterogeneous environment of live cells, a novel method was utilized to systematically correct for the different environmental effects on the fluorescence intensity of the probe when Bax occupies the cytosol or mitochondria (13), illustrated in Fig. 1. These corrections made it possible to identify how conformation of the C-terminal helix (α9) influences the accessibility of the BH3 domain as well as intracellular diffusion of Bax. In addition to recognizing intra-molecular changes in Bax associated with its insertion into the OMM, our measurements also detected inter-molecular contacts between separate Bax molecules isolated to specific helices. These observations not only identified the conformational changes Bax undergoes to commit to permeabilization of the OMM, but also the homo-oligomeric architecture Bax adopts when permeabilization occurs. Our findings have significant implications in evaluating molecular events involving Bax that have been proposed in triggering apoptosis.

EXPERIMENTAL PROCEDURES

Conjugation of FRET Pairs and Internal Reference to Bax Variants—Bax variants used to determine intra-molecular conformational changes contained two cysteines at specific locations. For one site, the wild-type residue at a particular position was mutated to a cysteine, whereas the native cysteine at residue 126 was changed to a serine. The other site utilized the wild-type cysteine at residue 62 in the BH3 domain. The same methods and protocols to conjugate the donor (Alexa Fluor 546), acceptor (Dabcyl), and internal reference (Alexa Fluor 633) to measure conformational changes between two wild-type cysteines 126 and 62 were employed in this study (13). To verify that the probes were conjugated at the different sites as well as the successful mutation to a cysteine, pepsin fragments of the reaction product and unreacted forms of these variants were analyzed by LC-MS. Microinjection was utilized to deliver conjugated Bax inside cells as described previously (13), where co-localization with MitoTracker Green verified translocation of Bax to the mitochondria (13). Cytochrome *c* release in cells that were microinjected with conjugated Bax was confirmed

(data not shown) to ensure that Bax translocation is followed by the normal apoptotic events.

To determine inter-molecular contacts using FRET, Bax variants containing a single cysteine were created. This was accomplished either by changing one of the wild-type cysteines (Cys^{62} or Cys^{126}) in Bax to a serine or by replacing both by serines and additionally modifying a non-cysteine residue to a cysteine. Then the same protocols were used to conjugate FRET probes as described previously (13). In these experiments the FRET donor would be on one Bax molecule, along with the internal reference, and the FRET acceptor would be on another Bax molecule. To ensure that there would always be a Bax molecule with an acceptor in proximity to a one with the donor in a scenario where they would be in contact, a 5:1 excess of Bax with the acceptor was mixed with Bax with the donor. This mixture was then microinjected into cells at a concentration of 300 nM. Previous estimates of the dilution of the solution resulting from microinjection are 1:10 (14). Using free dye, the estimated dilution for our settings was 1:5 to 1:10. Because the endogenous levels of Bax have been measured to be 2.7 to 3.7 nM, it is important to note that the resulting solution is still in $\times 10-20$ excess to the endogenous levels (15). Based on the distribution pattern of the fluorescence intensities before and after the addition of STS, the increased Bax cellular level did not seem to affect the translocation event. More importantly the effect of the relatively low level of endogenous protein to the measured FRET will be negligible.

To place the donor and acceptor at opposite ends of helix α6, Arg^{145} was replaced by a cysteine and Cys^{62} was changed to a serine, whereas cysteine at position 126 places a probe at the other end of this helix. The conjugation reaction to place the donor on these residues was only for 8 h instead of 17 to avoid having a donor on both cysteines. The purification protocols used to isolate the proper reaction product were identical as described before (13). Pepsin fragments analyzed by LC-MS confirmed the conjugation of the donor and acceptor to these locations.

Preparation of Bax with Intramolecular Cross-link between the C-terminal Helix and Helix α4—Some experiments required the C-terminal helix to be cross-linked to the core of Bax to verify FRET measurements obtained for this helix as well as to assist in analyzing the resulting intra-cellular diffusion. Cross-linking was performed between two lysines engineered into Bax utilizing the reactive *N*-hydroxysuccinimide ester groups on BS(PEG)5 (ThermoScientific). Although retaining the two cysteine residues that allow us to probe the C-terminal helix conformation, Cys^{62} and I175C mutant, Arg^{94} was changed to a lysine to cross-link with the wild-type Lys^{189}. To avoid cross-linking to the adjacent lysine, Lys^{190} was changed to an arginine. To cross-link R94K to Lys^{189}, this mutant was incubated at pH 7.0 in 0.1 M phosphate buffer and 6 mM Tris(2-carboxyethyl)phosphine for 3 h at room temperature in the presence of 15 mM BS(PEG)5. The reaction was stopped by buffer exchanging the reaction mixture into 20 mM Tris buffer, pH 8.0, using PD-10 columns (GE Healthcare). Reacted and unreacted forms of Bax were separated by a MonoQ column equilibrated with 20 mM Tris buffer, pH 8.0, using a 0–1 M NaCl gradient. To remove species that have been inter-molecularly cross-linked, the fractions that contained cross-linked Bax were eluted through a G-75 size-exclusion column and fractions that corresponded to monomeric Bax were pooled together to undergo conjugation with the FRET probes and internal reference. The following fragments from pepsin digestion verified cross-linking between R94K and Lys^{189}: fragments with residues 91–99 with 189–192 (1516.79 theoretical, 1516.78 experimental), 94–100 with 189–192 (1270.65 theoretical, 1270.65 experimental), and 93–98 with 189–192 (1139.61 theoretical, 1139.59 experimental).

Image Analysis and FRET Determination—The scheme to extract FRET efficiencies from the heterogeneous environment of a live cell is presented in Fig. 1. The fluorescent signals from Bax (F') conjugated with the FRET donor (Alexa Fluor 546) and the internal reference (Alexa Fluor 633) are measured in the cytosolic region of cells before and after the translocation of Bax. The systematic change in the fluorescent signal of the FRET donor (Alexa Fluor 546) that arises due to the migration from the diffuse cytosolic region to the membrane environment of the mitochondria is determined. Fluorescent signals in the region of the nucleus of cells were not included in the determination of FRET efficiencies. The fluorescent signals from another Bax molecule, F_Q', which contains the same FRET donor and internal reference in addition to the non-fluorescent FRET acceptor are also measured in the cytosolic regions of cells during translocation. FRET between the donor and acceptor is detected if there is a decrease in the donor fluorescence relative to the internal reference as detected in the sample, F', under the same conditions. The image analysis and subsequent treatment to extract FRET efficiencies were performed according to an earlier study (13).

Additional image analysis to allow rapid identification of possible FRET efficiencies was to use scatter plots to show correlations between the FRET donor and internal reference in the presence and absence of acceptor. After stacking images corresponding to the fluorescent signal of the donor and internal reference were prepared according to our previous work (13), a region of interest between 700 and 2300 pixels was selected in the cytosolic region of the cell. Then, two new images were created comprised of this region of interest for each channel. The "smoothing" function part of the program ImageJ was applied and the intensities were extracted from the XY coordinates of the image for each channel (16). The intensity of the donor *versus* internal reference at each coordinate was plotted and a correlation for each channel was observed. The scatter plots of samples with (F_Q') and without (F') the FRET acceptor were compared. The slope of this correlative trend would indicate the presence or absence of FRET. If the F_Q' sample gives a lower correlation slope relative to the F' sample, this indicates FRET. However, if these two samples have a correlation slope that is indistinguishable, no FRET is present. To quantify the FRET efficiency, a larger number of pixels representative over many cells were averaged using methods as described earlier (13). Typically our quantitative data sample was over 80,000 pixels. The standard deviation of the FRET efficiency was calculated by propagating errors in F' and F_Q' values measured from multiple cells (13).

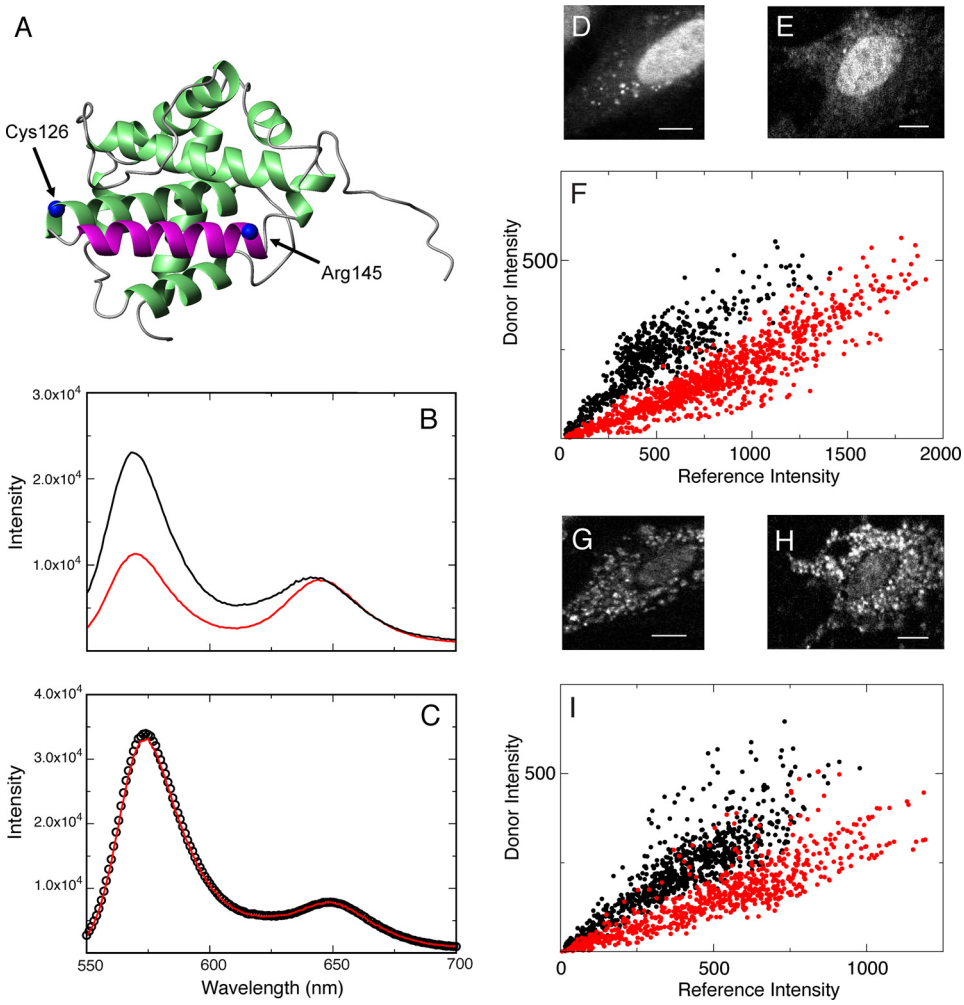

FIGURE 2. **Utilization of the C62S/R145C Bax mutant to determine whether the FRET pair Alexa Fluor 546-Dabcyl is sensitive to conformational changes during translocation from the cytosol to the mitochondria.** *A*, the FRET donor and acceptor were conjugated to Cys^{126} and R145C, which are at opposite ends of helix α6. *B*, fluorescence spectra of *F*′ (*black*) and F_Q′ (*red*) of this mutant in 20 mM Tris, pH 8. *C*, spectra of the same sample after the addition of 8 M guanidine HCl. *D*, an MEF cell microinjected with the *F*′ sample of this mutant before translocation. *E*, another MEF cell microinjected with the F_Q′ sample of this mutant before translocation. *F*, a scatter plot of the FRET donor (Alexa Fluor 546) and the reference (Alexa Fluor 633) intensities measured at individual pixels on the cells in *D* and *E* with (F_Q′, *red dots*, 1033 pixels, $r = 0.92$) and without (*F*′, *black dots*, 710 pixels, $r = 0.88$) the FRET acceptor (Dabcyl). *G*, the same cells as in *D*, which underwent translocation. *H*, the cell in *E*, which has undergone translocation. *I*, a scatter plot analysis, as described in *F*, but performed on cells in *G* and *H*. (*F*′, *black dots*, 742 pixels, $r = 0.88$; F_Q′, *red dots*, 749 pixels, $r = 0.87$). All scale bars are 10 μm.

FCS Measurements in Live Cells—Fluorescence correlation spectroscopy (FCS) was employed to analyze the intracellular diffusion of variants of Bax in the cytosolic regions of cells. These measurements were performed on a home-built system as described earlier (17). Rhodamine 6G and eGFP were utilized to calibrate and verify the instrument setup. Each time series acquisition was between 30 and 60 s. The number of curves acquired from a number of cells that comprises the final correlation curve in a figure is annotated. Igor software was used to fit these curves to one or two component three-dimensional diffusion model as described in earlier studies (18). The reported values and standard deviation of these fitted parameters is an average over the number of curves that comprise the final curve.

RESULTS

Justification for the Use of FRET between Alexa Fluor 546 and Dabcyl to Measure Distances in Two Different Intracellular Environments—The photochemical properties of the FRET pair of Alexa Fluor 546 and Dabcyl give rise to an R_0 of 29 Å, which makes it ideally suited to detect intra-molecular conformational changes in Bax. Because the environment could affect the properties of these probes, R_0 can also be affected. Therefore, in measuring changes in conformations that accompanies changes in environment, any effects on R_0, if any, that occur during translocation needed to be determined. This was done by attaching probes across a region of Bax at a distance roughly equal to R_0 that was known to retain its structure in a solution or membrane environment. If there were any changes to R_0, the measured FRET efficiency would be different under both conditions even if the probes were the same distance apart.

Previous investigations into the pore-forming activity of Bax showed that peptides that consisted of helices α5 and α6 retain their helicity and pore-forming activity (19, 20) in a membrane environment. Therefore the FRET donor and acceptor were placed at positions Cys^{126} and Arg^{145}, which spans helix α6 (Fig. 2*A*). The distance between the C_α carbons for these residues is 26 Å in the Bax structure (21). Fig. 2*B* shows that at 20 mM Tris, pH 8, FRET is detected between these two probes evidenced by

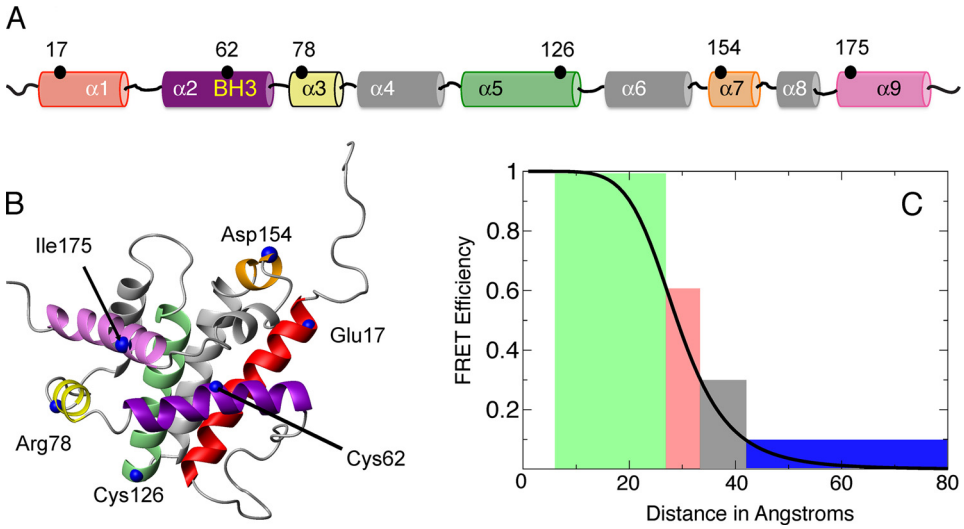

FIGURE 3. **Intra-molecular conformational changes in Bax were probed at distinct locations during translocation relative to the BH3 domain.** *A,* various residues that were modified to cysteine, where intra-molecular conformations were measured relative to Cys^{62} within the BH3 domain are shown in a linear fashion relative to helices in Bax. *B,* these mutations are represented on the NMR solution structure of Bax (PDB code 1F16). The helices are color coded in *A* and *B* similarly. *C,* the measured FRET efficiencies before and after translocation are categorized into four separate bins. They are displayed on the relationship curve between FRET efficiency and distance for the FRET pair Alexa Fluor 546 and Dabcyl. Efficiencies greater than 60% will be indicated as *green color*, those between 30 and 60% in *red*, those between 10 and 30% in *black*, and those less than 10% in *blue*.

the relative decrease in the fluorescence intensity at 570 nm from the donor Alexa Fluor 546, in the sample that contains the acceptor, F_Q', relative to the sample without it, F'. Both spectra were normalized to the fluorescent signal from the internal reference, Alexa Fluor 633, at 650 nm. The observed FRET efficiency of 0.50 corresponds to a distance of 29 Å, which is consistent with the distance between these two residues. However, Fig. 2*C* shows identical fluorescence spectra of F_Q' and F', which indicates an absence of FRET, when 8 M guanidine HCl was added to the buffer. Under this denaturing condition, there is no structure in Bax. Therefore, this FRET pair is a good reporter for an intact structure of helix α6. Any observed changes to the FRET efficiency between probes at these locations during translocation would reflect environmental changes to the R_0 of this pair and must be taken into account when interpreting a conformational change.

Fig. 2, *D* and *E,* show MEF cells microinjected with F' and F_Q' for this mutant, respectively. Each of these cells shows a diffuse distribution in the cytosolic region of Bax. Although there is a fluorescent signal around the nuclear region of these cells, this signal is not included in the determination of FRET efficiency during translocation. Interestingly, FRET efficiencies determined within this region are the same as the cytosolic values as long as the proper F' value (in this nuclear region) is compared with its corresponding F_Q' value. Fig. 2*F* shows a scatter plot of per-pixel intensities from the FRET donor and the fluorescent internal reference for the F' and F_Q' samples. A correlative trend can be seen in each of the plots of samples with and without the FRET acceptor. However, there is a lower correlation slope in the plot that contains the acceptor, which indicates the presence of FRET. The measured FRET efficiency detected at opposite ends of helix α6 before translocation (preSTS) is 0.49 ± 0.17, utilizing values of 0.41 ± 0.07 (8 cells) and 0.21 ± 0.06 (8 cells) for F' and F_Q', respectively. This value is close to 0.50 efficiency, determined from measurements in a 20 mM Tris, pH 8.0, buffer.

Fig. 2, *G* and *H*, show the same cells shown in *D* and *E*, except that the distribution of Bax is now punctate, resulting from the addition of STS. Similar to Fig. 2*F*, there is a correlation in the per-pixel intensities of the FRET donor and internal reference for both plots in Fig. 2*I*. In addition, there is also a lower slope to this trend for the plot that contains the acceptor, indicating the presence of FRET. After the translocation of Bax has occurred, the measured FRET efficiency is 0.50 ± 0.12, utilizing values of 0.80 ± 0.07 (8 cells) and 0.40 ± 0.06 (8 cells) for F' and F_Q', respectively, which is close to the efficiency determined before translocation.

The similar values of FRET efficiency measured before and after translocation, normalized to our internal reference, show that the R_0 value for this FRET pair is relatively unaffected by the change in environment in the cell. Therefore, distances can be extracted readily from FRET efficiencies before and after translocation without environmental correction.

Intra-molecular Conformational Changes That Accompany Translocation—The locations in Bax that were chosen to monitor intra-molecular conformational changes relative to the BH3 domain are shown in Fig. 3*A*. The FRET probes were conjugated site specifically to mutants of Bax as described under "Experimental Procedures." Fig. 3*B* shows the locations of these sites on the structure of Bax (21). According to distances obtained from this structure, FRET efficiency between probes at these sites relative to the BH3 domain should be detected. Any subsequent conformational changes would yield an increase or decrease in FRET efficiency. To simplify our data interpretation and considering the contribution from experimental noise, measured FRET efficiencies are characterized into distance segments shown as bins in Fig. 3*C*. The measured FRET efficiencies before and after translocation are shown in Table 1. An increase in the distance (or decrease in FRET efficiency) between helices α2-α1, α2-α5, and α2-α7 was observed. There is an observed increase in FRET efficiency between helices α2 and α3. Interestingly, we could not observe FRET

TABLE 1
Intra-molecular FRET efficiencies relative to Cys^{62} (α2)

	E′ − preSTS	E′ − postSTS
Glu^{17} − α1 (F', 15 cells; F_Q', 15 cells)	0.31 ± 0.16[a]	NF[b]
Arg^{78} − α3 (F', 14 cells; F_Q', 14 cells)	0.43 ± 0.15	0.67 ± 0.07
Cys^{126} − α5[c] (F', 16 cells; F_Q', 17 cells)	0.45 ± 0.14	0.11 ± 0.20
Asp^{154} − α7 (F', 12 cells; F_Q', 13 cells)	0.49 ± 0.09	NF
Ile^{175} − α9 (F', 15 cells; F_Q', 18 cells)	NF	NF

[a] Errors in FRET efficiency reported in this paper reflect the S.D. in the fluorescent intensity ratios.
[b] No FRET efficiency was detected between this position and Cys^{62} (α2).
[c] FRET efficiencies reported in Ref. 13.

between helices α2 and the C-terminal helix α9 (I175C) before and after translocation, even though a FRET efficiency of 0.70 was detected when Bax was incubated in a 20 mM Tris buffer, pH 8.0.

There is the possibility that the mutations and subsequent labeling of the Ile^{175} residue in the C-terminal helix affect the activity and cellular diffusion of Bax in live MEF cells. If this is true, then the observed FRET may not be representative of WT behavior. Image analysis of the translocation of this mutant compared with wild-type showed that this mutant exhibits the same transition from a diffuse to punctate distribution that accompanies translocation (Fig. 4), which also correlates with the observed FRET measurements. The FRET and morphological observations were confirmed by another mutant located on the same helix, T186C. In addition, the intracellular diffusion of these mutants was also compared with that of wild-type.

FCS was utilized to analyze the diffusive behavior of mutant and WT Bax in the cell. Fig. 5*A* shows FCS curves of eGFP, WT Bax, and I175C as well as T186C mutants of Bax. The measured diffusion constant for eGFP is 17 ± 3.7 μm^2/s. This is comparable with other values determined for HeLa (17), 22.5 ± 0.78 μm^2/s; COS-7 (22), 12.5 ± 1.3 μm^2/s; and MEF (23), 17.5 ± 1.3 μm^2/s, cells. The FCS curves for WT and mutant forms of Bax exhibit similar diffusive behavior before translocation. This demonstrates that the mutations and subsequent labeling of a FRET probe do not affect the intracellular diffusion relative to wild-type Bax in cells. Interestingly, these curves are different from FCS curves for eGFP. They could only be fit utilizing a two-component model. The diffusion constant of one component is similar to eGFP. For WT Bax and the I175C and T186C mutants, these constants are 10 ± 2.1, 10 ± 2.1, and 6 ± 2.2 μm^2/s, with a fractional population of 0.81 ± 0.05, 0.73 ± 0.08, and 0.78 ± 0.10, respectively. The other component is approximately 2 orders of magnitude slower. For WT Bax and the I175C and T186C mutants, these constants are 0.07 ± 0.026, 0.15 ± 0.078, and 0.05 ± 0.049 μm^2/s, with a fractional population of 0.19 ± 0.05, 0.27 ± 0.08, and 0.22 ± 0.10, respectively. This longer diffusive component is consistent with diffusion in organelles including membranes (18). Therefore, this shows that there is a population of Bax that resides in a membrane environment even before permeabilization of the OMM begins.

Previous studies have proposed that Bax can act as a catalyzer for insertion into the outer mitochondrial membrane (24). To determine whether endogenous Bax plays a role in affecting the relative population of this longer diffusive component, the intracellular diffusion of Bax in HCT116-WT and HCT116-Bax/Bak-DKO cells was measured using FCS. In both cell lines, Bax exhibited a two-component behavior as observed in the MEF cells. The fast diffusion component had the same order of magnitude as eGFP in the WT and DKO cell lines, 10 ± 10 and 25 ± 16 μm^2/s, respectively, with fractional populations of 0.84 ± 0.08 and 0.80 ± 0.08. The diffusion constants for eGFP in WT and DKO cells were 51 ± 22 and 47 ± 19 μm^2/s, respectively. In addition, there was a long phase component 2 orders of magnitude slower in WT and DKO cells, 0.03 ± 0.064 and 0.01 ± 0.014 μm^2/s, respectively, with fractional populations of 0.16 ± 0.08 and 0.20 ± 0.08. The similar intracellular diffusion of Bax in these cell lines demonstrates that it does not catalyze its transient contact with the mitochondria before translocation occurs.

Because it has been previously shown that the C-terminal helix is responsible for inserting into the OMM (25), we hypothesize that exposure of the C-terminal helix, as detected by our FRET measurements, is correlated with the slow diffusive behavior responsible for this longer diffusion component in the FCS curves of Bax. To test this, the C-terminal helix of Bax was cross-linked to the core of the protein. FCS was employed to analyze the intracellular diffusion rate of this form of Bax. FRET measurements at sites on the C terminus were also acquired to correlate the observed intracellular diffusion with conformations of this helix.

Fig. 5*B* shows the location of the cross-linked residues, Lys^{189} and R94K. The effect of this cross-link on the diffusion of Bax before translocation monitored by FCS is shown in Fig. 5*C*. The eGFP FCS curve from Fig. 5*A* is reproduced in this panel. Bax with the mutations necessary for the cross-linking but with the reaction not performed diffuses similarly to the wild-type. Whereas the same variant of Bax but cross-linked diffuses more like eGFP by reducing the population of the slow diffusing component from 0.34 to 0.16. This can be interpreted as a decrease in the amount of time that Bax interacts with a membrane. A FRET efficiency of 0.38 ± 0.08, utilizing values of 1.82 ± 0.13 (6 cells) and 1.14 ± 0.13 (11 cells) for F' and F_Q', respectively, is measured between I175C on the C-terminal helix and Cys^{62} on the BH3 domain, which was not present without cross-linking the C-terminal helix. This demonstrates that an exposed C-terminal helix is responsible for the population of Bax that interacts with a membrane environment before translocation. The effect of this cross-link after the addition of STS is shown in Fig. 5*D*. The autocorrelation curve of the mutant variant of Bax that does not have a cross-link shows a diffusive behavior of a protein associated with a large organelle, consistent with wild-type behavior. However, the same variant protein that is cross-linked diffuses similarly as a protein in the cytosol. It has been previously shown that Bax molecules were not observed to translocate with a truncated C terminus (25). This further supports that the exposure of the C-terminal helix not only in the membrane but also in the cytosol is necessary for the biological activity of Bax.

Because the observation of this longer diffusive component shows that Bax is ready to insert into the OMM, we tested whether the BH3 mimetic ABT-737 can affect the structure or intracellular diffusion of Bax to more efficiently undergo trans-

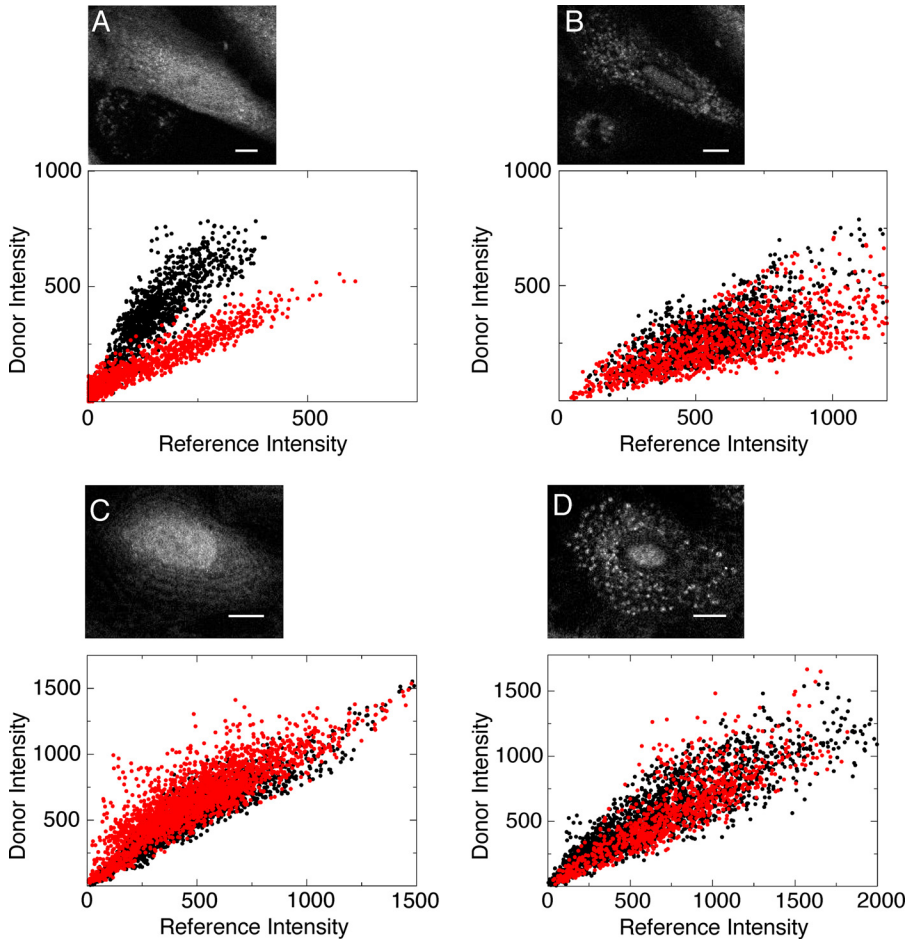

FIGURE 4. **Mutations and subsequent conjugations to the C terminus of Bax do not affect its activity inside cells.** *A,* scatter plots of the FRET donor and the reference intensities from wild-type Bax microinjected into an MEF cell measured at individual pixels. The lower correlative slope of the sample with the donor (F_Q', *red dots*, 865 pixels, $r = 0.94$) compared with the sample without it (F', *black dots*, 1091, $r = 0.86$) indicates FRET between positions Cys^{126} and Cys^{62}. The *inset* shows an MEF cell microinjected with Bax and has a diffuse distribution. *B,* scatter plots from labeled wild-type Bax that has undergone translocation. Unlike the scatter plots in *A*, the similar correlative slopes of the samples with and without the acceptor, F_Q' (*red dots*, 1203 pixels, $r = 0.76$) and F' (*black dots*, 1380, $r = 0.69$), respectively, indicate a loss of FRET efficiency between Cys^{126} and Cys^{62}. The *inset* shows the same MEF cell in *A* that has undergone translocation, where microinjected Bax now has a punctate distribution. *C,* scatter plot analysis of the C126S/I175C mutant of Bax before translocation. The similar correlative slopes of the samples with and without the acceptor, F_Q' (*red dots*, 2293 pixels, $r = 0.87$) and F' (*black dots*, 2062 pixels, $r = 0.93$), respectively, show that there is no FRET between the probes on the BH3 domain and helix α9. Although this efficiency corresponds to this helix being exposed to the solvent and thus has the ability to associate with a membrane environment, it still maintains a diffuse distribution in the cytosol seen in the *inset* as compared with the wild-type distribution in *A*. *D,* scatter plot analysis of the C126S/I175C mutant of Bax after translocation. The scatter plots of samples with and without the acceptor, F_Q' (*red dots*, 921 pixels, $r = 0.86$) and F' (*black dots*, 2248 pixels, $r = 0.91$), respectively, have the same correlation slope, which shows that there is no FRET between the probes on the BH3 domain and helix α9 when inserted into the OMM. As seen in the *inset*, the distribution of this mutant of Bax is now punctate, similar to the distribution of wild-type Bax seen in *B*. All *scale bars* are 10 μm.

location. Although an increase in the incidence of translocation was observed when 10 μM ABT-737 was added in tandem with 3.6 μM STS (86 ± 14% cells in which Bax was translocated in 75 min, in two independent experiments, 43 cells total) compared with only STS (41 ± 9% cells in which Bax was translocated in 75 min, in two experiments, 43 cells total), the FRET efficiency between Cys^{126} and Cys^{62} was the same with ABT-737, 0.42 ± 0.28, or without it, 0.45 ± 0.14, added along side with STS. No cells showed Bax translocation within this time in the presence of only ABT-737. In addition, the relative population of the fast component of the FCS curves remains similar in the presence of ABT-737, 86 ± 14% (4 curves; 3 cells), or its absence, 81 ± 5% (8 curves; 3 cells). Therefore, we hypothesize that ABT-737 increases the instance of translocation of Bax through interactions at the OMM possibly with other partners. This is consistent with previous observations that ABT-737 binds to the BH3 domain of Bcl-xL (26) thus possibly exposing its C terminus, which is responsible for keeping Bax out of the mitochondria before translocation occurs (12).

When Bax commits to translocation, the FRET efficiencies measured to helices α1, α5, α7, and α9 relative to the BH3 domain correspond to distances greater than 40 Å according to Table 1 and Fig. 3*C*. This indicates that Bax is adopting a more extended structure. However, the FRET efficiency to helix α3 increased. Two scenarios can account for this observation: (i) Bax adopts a conformation that brings helix α3 closer to the BH3 domain or (ii) another Bax molecule that contains the acceptor is close enough to helix α3 that allows inter-molecular FRET to also occur.

Inter-molecular Contacts Formed as a Result of Translocation—To determine whether the increase in the intra-molecular FRET in helix α3 could have an inter-molecular contri-

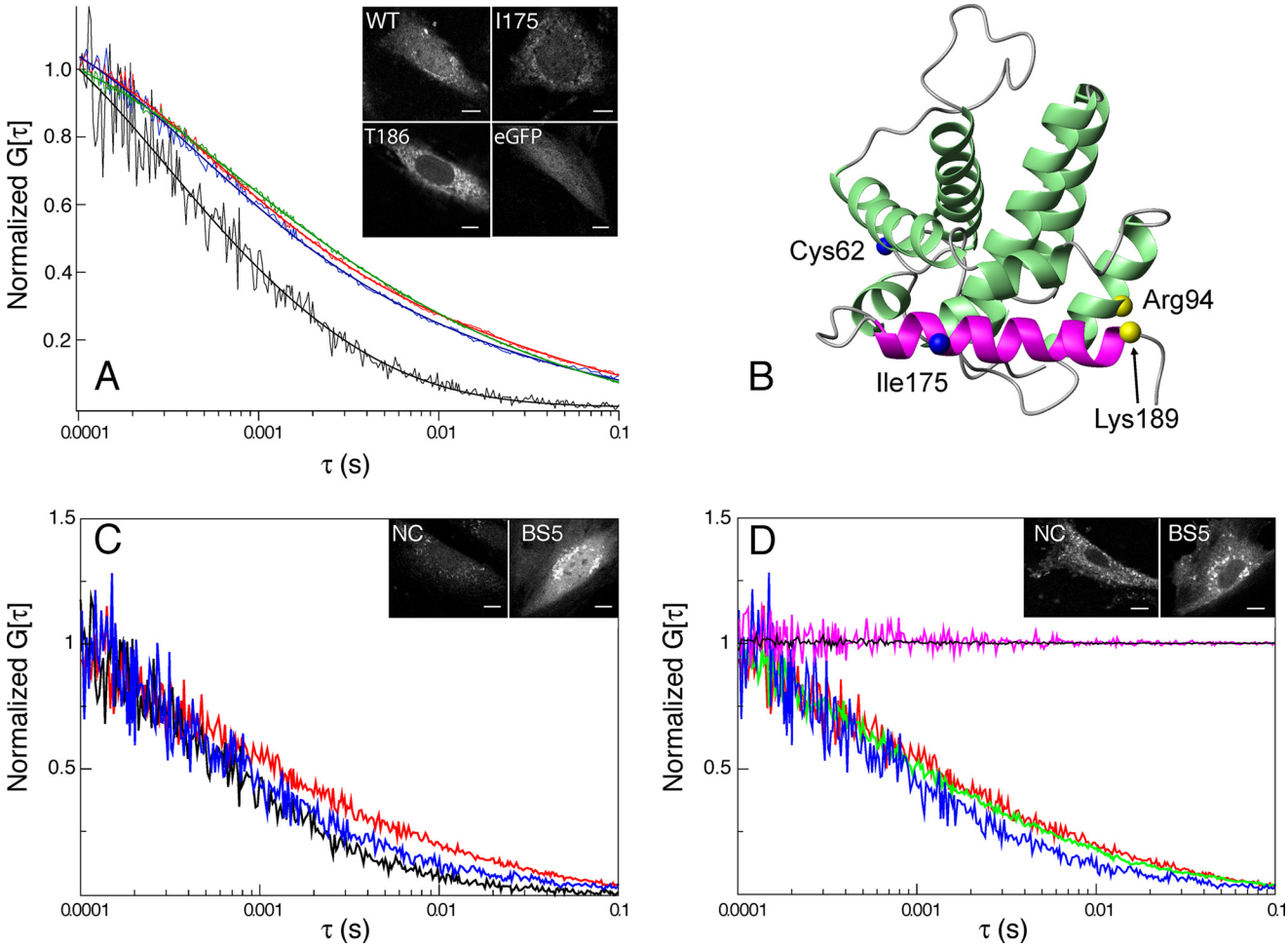

FIGURE 5. **Determining intracellular diffusion using FCS.** *A,* FCS curves for eGFP (*black*, 8 curves over 3 cells), WT Bax (*red*, 8 curves over 3 cells), C126S/I175C mutant Bax (*green*, 8 curves over 3 cells), and C126S/T186C mutant Bax (*blue*, 8 curves over 3 cells) before the addition of STS are shown as a function of the correlation time. *B,* the Cα atoms of the residues used to cross-link helices α9 to α4 using BS(PEG)5 are shown as *yellow spheres*. Arg[94] was mutated to a lysine to utilize *N*-hydroxysuccinimide ester groups to carry out the cross-linking. *C,* FCS curves of eGFP (*black*, 8 curves over 3 cells), cross-linked R94K mutant Bax, BS5 (*blue*, 15 curves, 5 cells), and R94K mutant Bax with no cross-linking, NC (*red*, 15 curves over 5 cells) before translocation. *D*, FCS curves of cross-linked Bax, BS5, before (*blue*) and after (*green*, 9 curves over 3 cells) STS was added, as well as, non-cross-linked Bax, NC, before (*red*) and after (*magenta*, 9 curves over 3 cells) STS was added. The FCS curve of WT Bax after the addition of STS is also shown (*black*, 9 curves over 3 cells).

bution, the F_Q' sample was used to microinject into MEF cells comprised of two distinct species of Bax. One species of Bax contained the donor conjugated on helix α3 and the internal reference and the other species only contained the acceptor conjugated at the BH3 domain on Cys[62]. Fig. 6 shows scatter plot analysis similar to Figs. 2 and 4 between these two sites. The lower correlation slope of the F_Q' sample indicates inter-molecular FRET between the donor and acceptor. Inter-molecular FRET efficiency was detected between these two sites to be 0.44 ± 0.12. Therefore, the observed FRET efficiency for this site has an inter-molecular as well as an intra-molecular component. When the inter-molecular contribution is subtracted from the total FRET efficiency observed for this site, 0.67 ± 0.07, the resulting efficiency, 0.23, yields a decrease in the intra-molecular FRET efficiency from 0.43. This indicates that helix α3 moves away from the BH3 domain as a result of translocation. Inter-molecular FRET efficiencies were also acquired between sites on helices on different Bax molecules and are summarized in Table 2. As a negative control scatter plot analysis for Bax mutants used to probe intermolecular contacts, listed in Table 2, before translocation are shown in Fig. 6, *A*, *C*, and *E*. No FRET between different Bax molecules was detected before translocation occurred.

DISCUSSION

Before the Commitment to OMM Permeabilization—A representation of the conformational changes before and after translocation observed from the FRET measurements listed in Table 1 and classified using the bins in Fig. 3*C* is shown in Fig. 7*A*. For helices α1, α3, α5, and α7, the measured FRET efficiencies before translocation correspond to distances consistent with the NMR structure of Bax (21). Therefore, the arrangement of the helices in Fig. 7*A* is similar to this structure. However, the efficiency measured to helix α9 corresponds to a distance that is greater than 45 Å, which suggests that the C-terminal helix is exposed to the cellular environment. According to the published structure, this helix is tucked into the core of the protein. It is important to note that due to our experimental error, a 15% or less population of the protein with the C-terminal helix packed against the core would not be

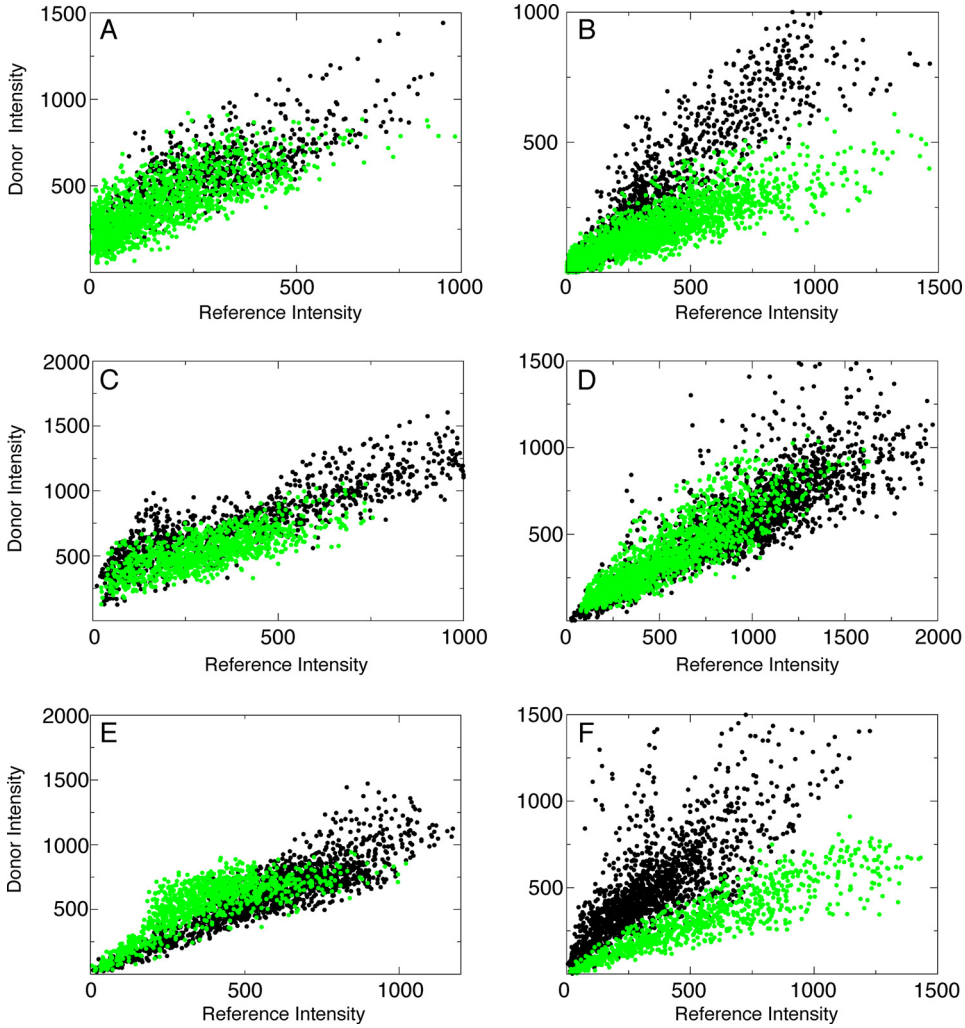

FIGURE 6. **Intermolecular FRET between helices after translocation.** Scatter plot analysis of the intensities of the donor and acceptor on individual pixels in the absence (*F′*, *black dots*) and presence (F_Q', *green dots*) of another protein co-injected into cells that contains only the acceptor. *A,* no FRET is detected between helix α3 at position 78 on one Bax molecule and helix α2 at position 62 on another molecule before translocation as evidenced by the same correlation slope when protein with the acceptor is co-injected (*F′*, *black dots*, 1239 pixels, $r = 0.86$; F_Q', *green dots*, 2168 pixels, $r = 0.75$). *B,* after translocation, FRET is detected between the two sites in *A* evidenced by the lower correlation slope of the sample that contains the FRET acceptor (*F′*, *black dots*, 1049 pixels, $r = 0.87$; F_Q', *green dots*, 1720 pixels, $r = 0.87$). *C,* there is no contact between helix α5 on separate molecules before translocation evidenced by similar correlation slopes in the presence and absence of the acceptor, which also indicates no FRET (*F′*, *black dots*, 1053 pixels, $r = 0.89$; F_Q', *green dots*, 1405 pixels, $r = 0.75$). *D,* no contact between the sites in *C* are observed after translocation evidenced by the same correlation slope between the samples with and without the FRET acceptor (*F′*, *black dots*, 1405 pixels, $r = 0.84$; F_Q', *green dots*, 1668 pixels, $r = 0.87$). *E,* no intermolecular contact between helix α9 on separate Bax molecules is observed before translocation evidenced by the same correlation slope between samples with and without the FRET acceptor (*F′*, *black dots*, 1367 pixels, $r = 0.90$; F_Q', *green dots*, 887 pixels, $r = 0.79$). *F,* intermolecular contacts are observed between the sites in *E* evidenced by the lower correlation slope of the sample with the FRET acceptor (*F′*, *black dots*, 1487 pixels, $r = 0.78$; F_Q', *green dots*, 825 pixels $r = 0.91$).

TABLE 2

Inter-molecular FRET efficiencies

	E′ − postSTS
Glu^{17}:Glu^{17} (*F′*, 13 cells; F_Q', 15 cells)	NF[a]
Arg^{78}:Cys^{62} (*F′*, 14 cells; F_Q', 13 cells)	0.44 ± 0.12
Cys^{62}:Cys^{62} (*F′*, 14 cells; F_Q', 13 cells)	0.20 ± 0.20
Arg^{78}:Arg^{78} (*F′*, 8 cells; F_Q', 8 cells)	NF
Cys^{126}:Cys^{126} (*F′*, 11 cells; F_Q', 9 cells)	NF
Arg^{145}:Arg^{145} (*F′*, 15 cells; F_Q', 14 cells)	NF
Ile^{175}:Ile^{175} (*F′*, 12 cells; F_Q', 15 cells)	0.41 ± 0.20
Thr^{186}:Thr^{186} (*F′*, 10 cells; F_Q', 10 cells)	0.54 ± 0.15
Ile^{175}:Thr^{186} (*F′*, 12 cells; F_Q', 13 cells)	0.08 ± 0.20

[a] No intermolecular FRET was detected between these sites.

detected. In Fig. 7*B*, the measured FRET efficiencies after translocation for helices α1, α5, α7, and α9 decrease to less than 15%. This shows that Bax adopts extended conformation(s) when it commits to the permeabilization of the OMM. Only one site on helix α3 shows an increase in FRET efficiency to greater than 60%.

The exposure of the C-terminal helix as well as its intracellular diffusion measured by FCS are consistent with the model that Bax is in a dynamic equilibrium between the cytosol (10–12) and the mitochondria. This exposure allows Bax to be poised to insert into the mitochondria and this helix has been shown previously to be responsible for membrane insertion (25). The FCS curves show that there is a population of Bax that transiently interacts with an organelle, before translocation. This population goes away when helix α9 is cross-linked to helix α4.

Bax adopting conformations in which the C-terminal helix is exposed in the cytosol is indicative of a more complex environment of the cell than a dilute buffer. We also did not observe

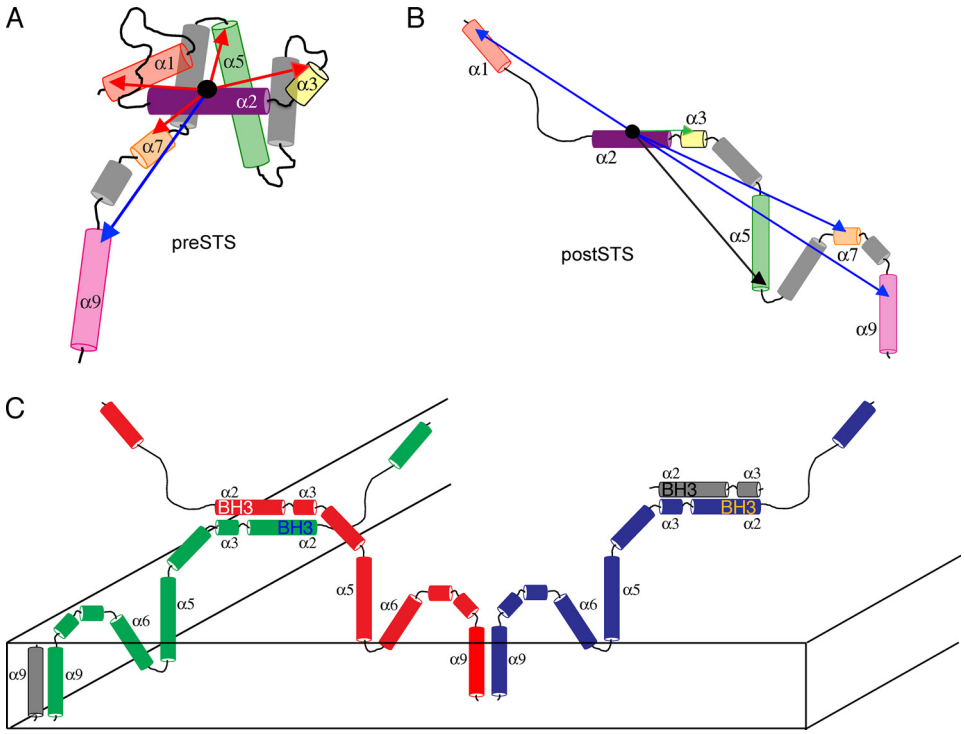

FIGURE 7. **Models for the conformational changes that occur in Bax as a result of translocation and the inter-molecular contacts formed in the OMM.** *A,* FRET efficiencies of Bax determined before translocation, taken from Table 1 and colored according to the bins as described in the legend to Fig. 3*C*, are illustrated on a proposed model of Bax where the C-terminal helix α9 is exposed. Of the five efficiencies, four correspond to distances that are consistent with the NMR solution structure of Bax. *B,* FRET efficiencies determined after translocation, taken from Table 1. *C,* two sites of inter-molecular contact are shown between the BH3 domains of separate Bax molecules as well as between C-terminal helices. The absence of FRET between helices α5 and α6 implies that an oligomeric rather than a dimer architecture is a reasonable model to satisfy these contacts.

inter-molecular FRET efficiencies between Bax molecules in the cytosol. It is still unclear from this study what is responsible for establishing this conformation. It is very unlikely that the observed cytosolic conformation can be present without any other factors interacting with Bax to promote and stabilize the opening of the C-terminal helix. Although this hypothesis might be contradictory to a previous study (27) that showed that no additional factors are necessary for Bax to interact with a lipid membrane, interestingly a pull-down assay did identify a heat shock protein to be isolated with Bax (28). It is well established that heat shock proteins are crucial in destabilizing substrate proteins for unfolding prior to recognition by membrane acceptor or transporter. Perhaps the heat shock protein can play a role in destabilizing the C-terminal helix of Bax for targeting the mitochondria membrane. Although the helix α9 is exposed for Bax to enter the mitochondria, the total population does not insert. One explanation for this is that Bcl-x_L is interacting with Bax and retrotranslocating it back into the cytosol as part of the dynamic equilibrium between the cytosol and mitochondria (10, 12). Previous studies determined that the rate of retrotranslocation is on the order of 100 s. The slow phase detected in this study is on the order of 0.1 s. Therefore, within the time scale of our FCS measurements, the rate of translocation does not affect the measured correlation time of the slower phase. Most likely, we are observing both the major cytosolic and minor mitochondria populations of Bax within our FCS measurement whose relative population could be tuned by its interaction with Bcl-x_L. Previous work has shown that interactions with Bcl-x_L and the BH3 domain of Bax may be responsible for this distribution (8, 29). Indeed, exposure of the C-terminal helix increases the potential access to this domain. In fact, a model of a complex between Bcl-x_L and Bax trapped in a membrane environment has been proposed in which Bcl-x_L makes contacts with the BH3 domain of Bax (30) with its C-terminal helix exposed. Our results suggest that this interaction might occur even earlier, prior to membrane insertion.

Contacts Involved in Permeabilizing the OMM That Continue the Onset of Apoptosis—When a cell finally commits to apoptosis and Bax has undergone translocation to the OMM, the characteristic structural change that Bax undergoes is to adopt an extended conformation. This allows Bax to form inter-molecular interactions and the possibility to interact with other proteins and factors as apoptotic pores are formed in the OMM. This is the first study to acquire distance information to specific helices in full-length Bax inside live cells during this process.

In this extended conformation, inter-molecular contacts were observed between separate Bax molecules. One site of interaction was at their C-terminal helices as shown in Fig. 7*C*. The interaction may be critical to the commitment to OMM permeabilization, because whereas our FCS data indicated that it could interact with a membrane environment, inter-molecular contact between C-terminal helices was only detected after translocation has occurred. Another site where inter-molecular contacts were detected was at the BH3 domains of separate Bax molecules. This interaction also signals a commitment to OMM permeabilization. Until translocation is triggered, this domain is sequestered by the other helices in Bax. However, in

the OMM, in the extended conformation, it forms contacts with another Bax molecule. Although previous studies that utilize isolated mitochondrial complexes (31) or liposomes (32) propose an interaction between the BH3 domains, our study directly identifies this dimerization interface in live cells as the permeabilization of the OMM is occurring. Although our confirmation of the presence of this interaction as the content of mitochondrial membranes are changing and additional factors influence its morphology is important, we went further and determined additional distances to the other helices relative to this domain so that we can build a physiological model of Bax embedded in the OMM.

A schematic for the arrangement of inter-molecular contacts between different Bax molecules after translocation is shown in Fig. 7*C*. One assumption that is made is that helices are intact although embedded in the OMM. This is reasonable because it has been shown previously that helices α5, α6, and α9 retain their helical character in model membranes (20, 33). In addition, these helices were shown to be embedded in the OMM (34), and is depicted in Fig. 7*C*. Although there remains critical information to be gathered to render an accurate structure, including how these helices are packed in the membrane environment and their relative orientation, inferences about their arrangement can be made from the intra- and inter-molecular FRET efficiencies that were measured. The efficiency between the Arg^{78} and Cys^{62} sites on different Bax molecules places helices α2 and α3 in proximity. The anti-parallel nature of these helices is assumed due to the lower efficiency between BH3 helices at position Cys^{62}, 0.20 ± 0.20, as well as the lack of detection of efficiency between Arg^{78} residues. The C-terminal helices on different Bax molecules are placed in proximity due to the observed efficiency on two sites on this helix. A FRET efficiency of 0.41 ± 0.20 was observed between the Ile^{175} sites on two Bax molecules. Similarly, an efficiency of 0.54 ± 0.20 was observed between the Thr^{186} sites. In Fig. 7*C*, we propose that these helices are arranged in a parallel orientation due to the lower efficiency detected between positions Ile^{175} and Thr^{186}, 0.08 ± 0.20. The absence of FRET between the Cys^{126} and Arg^{145} sites on different Bax molecules makes it reasonable to assume that more than two Bax molecules must be responsible for contacts at the C terminus and BH3 domain. The absence of FRET means that the helices that contain these sites cannot be less than 50 Å from each other. Realistically, there are not enough helices within a Bax molecule to wrap around this void to contact both the C terminus and BH3 domain, especially if helices α5 and α6 retain their helicity. The extended configuration formulated from these FRET efficiencies also allows for other proteins and factors to interact with Bax to commit cells to undergo apoptosis.

Another phenomenon that has been observed with the translocation of Bax is oligomerization in the OMM as apoptotic pores are formed (35). Although the number of Bax molecules per pore was not determined, Fig. 7*C* presents the two distinct sites of inter-molecular contact to form homo-oligomers. An alternative site for oligomerization has been proposed that is different from the one presented here (31). It is at helix α6 on separate Bax molecules. However, in this present study, no inter-molecular FRET was detected at the two ends of this helix. Because the FRET efficiencies presented here were acquired in the cellular environment, the schematic presented in Fig. 7*C* would be more representative of the physiological condition, which can include many components. These may include other Bcl-2 proteins (35) or lipids (9). The extended structure of Bax in this oligomeric state does not preclude this possibility.

Using a novel technique to extract distance information in live cells allowed us to determine key structural elements in Bax that affect the regulation of the permeabilization of the OMM. We were able to distinguish three different populations of Bax: cytosolic, membrane-associated, and membrane-embedded. The observation of an exposed C-terminal helix based on our FRET measurements, possibly due to a cytosolic factor, allows for the interactions of Bax with the mitochondria membrane. These two populations that correspond to cytosolic and membrane-associated Bax were detected by FCS. Although associated with the mitochondria it can interact with Bcl-x_L through their C-terminal helices (12) to retrotranslocate back into the cytosol. When apoptosis was triggered with STS, the mitochondria-associated Bax is activated through "hit-and-run" interactions with its BH3 domain and tBid or BIM to undergo conformational changes to commit to insertion in the OMM (36). A consequence of this activation is exposing helices α5 and α6 from the BH3 to embed in the OMM, which was observed by a loss of FRET efficiency between these two sites. Bax has "switched" from a compact structure to an extended one. This conformational "switch" is not reversible. This membrane embedded population is stabilized by forming inter-molecular interactions between its BH3 domains and C-terminal helices, which were also detected using FRET. These contacts form an oligomeric architecture that can permeabilize the OMM or where potentially other Bcl-2 proteins can associate with Bax to enhance this process. Identifying where other proteins interact with Bax will uncover more details of the regulatory mechanism of the Bcl-2 family of proteins.

Acknowledgments—We are deeply indebted to Ephrem Tekle for technical support and guidance. We also acknowledge Motoshi Suzuki for helpful discussion and suggestions, Grzegorz Piszczek of the NHLBI Biophysical Core Facility, and Duck-Yeon Lee of the NHLBI Biochemical Facility, Richard J. Youle of NINDS for the HCT116-WT and HCT116-Bax/Bak-DKO cells, and Chunxin Wang and David Bacsik for technical assistance.

REFERENCES

1. Czabotar, P. E., Lessene, G., Strasser, A., and Adams, J. M. (2014) Control of apoptosis by the BCL-2 protein family: implications for physiology and therapy. *Nat. Rev. Mol. Cell Biol.* **15,** 49–63
2. Sassone, J., Maraschi, A., Sassone, F., Silani, V., and Ciammola, A. (2013) Defining the role of the Bcl-2 family proteins in Huntington's disease. *Cell Death Dis.* **4,** e772
3. Green, D. R. (2004) The pathophysiology of mitochondrial cell death. *Science* **305,** 626–629
4. Cory, S., and Adams, J. M. (2002) The bcl2 family: regulators of the cellular life-or-death switch. *Nat. Rev. Cancer.* **2,** 647–656
5. Tait, S. W., and Green, D. R. (2013) Mitochondrial regulation of cell death. *Cold Spring Harb. Perspect. Biol.* **5,** a008706–a008706
6. Kelly, P. N., and Strasser, A. (2011) The role of Bcl-2 and its pro-survival relatives in tumourigenesis and cancer therapy. *Cell Death Differ.* **18,** 1414–1424

7. Youle, R. J., and Strasser, A. (2008) The BCL-2 protein family: opposing activities that mediate cell death. *Nat. Rev. Mol. Cell Biol.* **9,** 47–59
8. Fletcher, J. I., Meusburger, S., Hawkins, C. J., Riglar, D. T., Lee, E. F., Fairlie, W. D., Huang, D. C., and Adams, J. M. (2008) Apoptosis is triggered when prosurvival Bcl-2 proteins cannot restrain Bax. *Proc. Natl. Acad. Sci. U.S.A.* **105,** 18081–18087
9. García-Sáez, A. J. (2012) The secrets of the Bcl-2 family. *Cell Death Differ.* **19,** 1733–1740
10. Edlich, F., Banerjee, S., Suzuki, M., Cleland, M. M., Arnoult, D., Wang, C., Neutzner, A., Tjandra, N., and Youle, R. J. (2011) Bcl-xL retrotranslocates Bax from the mitochondria into the cytosol. *Cell* **145,** 104–116
11. Schellenberg, B., Wang, P., Keeble, J. A., Rodriguez-Enriquez, R., Walker, S., Owens, T. W., Foster, F., Tanianis-Hughes, J., Brennan, K., Streuli, C. H., and Gilmore, A. P. (2013) Bax exists in a dynamic equilibrium between the cytosol and mitochondria to control apoptotic priming. *Mol. Cell* **49,** 959–971
12. Todt, F., Cakir, Z., Reichenbach, F., Youle, R. J., and Edlich, F. (2013) The C-terminal helix of Bcl-xL mediates Bax retrotranslocation from the mitochondria. *Cell Death Differ.* **20,** 333–342
13. Gahl, R. F., Tekle, E., and Tjandra, N. (2014) Single color FRET based measurements of conformational changes of proteins resulting from translocation inside cells. *Methods* **66,** 180–187
14. Pepperkok, R., Scheel, J., Horstmann, H., Hauri, H. P., Griffiths, G., and Kreis, T. E. (1993) β-COP is essential for biosynthetic membrane transport from the endoplasmic reticulum to the Golgi complex *in vivo*. *Cell* **74,** 71–82
15. Polster, B. M., Basañez, G., Young, M., Suzuki, M., and Fiskum, G. (2003) Inhibition of Bax-induced cytochrome *c* release from neural cell and brain mitochondria by dibucaine and propranolol. *J. Neurosci.* **23,** 2735–2743
16. Schneider, C. A., Rasband, W. S., and Eliceiri, K. W. (2012) NIH Image to ImageJ: 25 years of image analysis. *Nat. Methods* **9,** 671–675
17. Lazarou, M., Narendra, D. P., Jin, S. M., Tekle, E., Banerjee, S., and Youle, R. J. (2013) PINK1 drives Parkin self-association and HECT-like E3 activity upstream of mitochondrial binding. *J. Cell Biol.* **200,** 163–172
18. Haustein, E., and Schwille, P. (2003) Ultrasensitive investigations of biological systems by fluorescence correlation spectroscopy. *Methods* **29,** 153–166
19. García-Sáez, A. J., Coraiola, M., Serra, M. D., Mingarro, I., Müller, P., and Salgado, J. (2006) Peptides corresponding to helices 5 and 6 of Bax can independently form large lipid pores. *FEBS J.* **273,** 971–981
20. García-Sáez, A. J., Coraiola, M., Dalla Serra, M., Mingarro, I., Menestrina, G., and Salgado, J. (2005) Peptides derived from apoptotic Bax and Bid reproduce the poration activity of the parent full-length proteins. *Biophys. J.* **88,** 3976–3990
21. Suzuki, M., Youle, R. J., and Tjandra, N. (2000) Structure of Bax: coregulation of dimer formation and intracellular localization. *Cell* **103,** 645–654
22. Wachsmuth, M., Waldeck, W., and Langowski, J. (2000) Anomalous diffusion of fluorescent probes inside living cell nuclei investigated by spatially-resolved fluorescence correlation spectroscopy. *J. Mol. Biol.* **298,** 677–689
23. Lidke, D. S., Huang, F., Post, J. N., Rieger, B., Wilsbacher, J., Thomas, J. L., Pouysségur, J., Jovin, T. M., and Lenormand, P. (2010) ERK nuclear translocation is dimerization-independent but controlled by the rate of phosphorylation. *J. Biol. Chem.* **285,** 3092–3102
24. Bellot, G., Cartron, P.-F., Er, E., Oliver, L., Juin, P., Armstrong, L. C., Bornstein, P., Mihara, K., Manon, S., and Vallette, F. M. (2007) TOM22, a core component of the mitochondria outer membrane protein translocation pore, is a mitochondrial receptor for the proapoptotic protein Bax. *Cell Death Differ.* **14,** 785–794
25. Wolter, K. G., Hsu, Y. T., Smith, C. L., Nechushtan, A., Xi, X. G., and Youle, R. J. (1997) Movement of Bax from the cytosol to mitochondria during apoptosis. *J. Cell Biol.* **139,** 1281–1292
26. Lee, E. F., Czabotar, P. E., Smith, B. J., Deshayes, K., Zobel, K., Colman, P. M., and Fairlie, W. D. (2007) Crystal structure of ABT-737 complexed with Bcl-xL: implications for selectivity of antagonists of the Bcl-2 family. *Cell Death Differ.* **14,** 1711–1713
27. Yethon, J. A., Epand, R. F., Leber, B., Epand, R. M., and Andrews, D. W. (2003) Interaction with a membrane surface triggers a reversible conformational change in Bax normally associated with induction of apoptosis. *J. Biol. Chem.* **278,** 48935–48941
28. Vogel, S., Raulf, N., Bregenhorn, S., Biniossek, M. L., Maurer, U., Czabotar, P., and Borner, C. (2012) Cytosolic Bax: does it require binding proteins to keep its pro-apoptotic activity in check? *J. Biol. Chem.* **287,** 9112–9127
29. Czabotar, P. E., Lee, E. F., Thompson, G. V., Wardak, A. Z., Fairlie, W. D., and Colman, P. M. (2011) Mutation to Bax beyond the BH3 domain disrupts interactions with pro-survival proteins and promotes apoptosis. *J. Biol. Chem.* **286,** 7123–7131
30. Ding, J., Mooers, B. H., Zhang, Z., Kale, J., Falcone, D., McNichol, J., Huang, B., Zhang, X. C., Xing, C., Andrews, D. W., and Lin, J. (2014) After embedding in membranes antiapoptotic Bcl-XL protein binds both Bcl-2 homology region 3 and helix 1 of proapoptotic Bax protein to inhibit apoptotic mitochondrial permeabilization. *J. Biol. Chem.* **289,** 11873–11896
31. Dewson, G., Ma, S., Frederick, P., Hockings, C., Tan, I., Kratina, T., and Kluck, R. M. (2012) Bax dimerizes via a symmetric BH3:groove interface during apoptosis. *Cell Death Differ.* **19,** 661–670
32. Bleicken, S., Classen, M., Padmavathi, P. V., Ishikawa, T., Zeth, K., Steinhoff, H. J., and Bordignon, E. (2010) Molecular details of Bax activation, oligomerization, and membrane insertion. *J. Biol. Chem.* **285,** 6636–6647
33. Tatulian, S. A., Garg, P., Nemec, K. N., Chen, B., and Khaled, A. R. (2012) Molecular basis for membrane pore formation by Bax protein carboxyl terminus. *Biochemistry* **51,** 9406–9419
34. Annis, M. G., Soucie, E. L., Dlugosz, P. J., Cruz-Aguado, J. A., Penn, L. Z., Leber, B., and Andrews, D. W. (2005) Bax forms multispanning monomers that oligomerize to permeabilize membranes during apoptosis. *EMBO J.* **24,** 2096–2103
35. Westphal, D., Kluck, R. M., and Dewson, G. (2014) Building blocks of the apoptotic pore: how Bax and Bak are activated and oligomerize during apoptosis. *Cell Death Differ* **21,** 196–205
36. Walensky, L. D., and Gavathiotis, E. (2011) BAX unleashed: the biochemical transformation of an inactive cytosolic monomer into a toxic mitochondrial pore. *Trends Biochem. Sci.* **36,** 642–652